Geocarto International

ISSN: 1010-6049 (Print) 1752-0762 (Online) Journal homepage: https://www.tandfonline.com/loi/tgei20

Investigating flash floods potential areas using ASCAT and TRMM satellites in the Western Cape Province, South Africa

Tsitsi Bangira, Ben H.P. Maathuis, Timothy Dube & Tawanda W. Gara

To cite this article: Tsitsi Bangira, Ben H.P. Maathuis, Timothy Dube & Tawanda W. Gara (2015) Investigating flash floods potential areas using ASCAT and TRMM satellites in the Western Cape Province, South Africa, Geocarto International, 30:7, 737-754, DOI: 10.1080/10106049.2014.997302

To link to this article: https://doi.org/10.1080/10106049.2014.997302

Geocarto International, 2015
Vol. 30, No. 7, 737–754, http://dx.doi.org/10.1080/10106049.2014.997302

Taylor & Francis
Taylor & Francis Group

Investigating flash floods potential areas using ASCAT and TRMM satellites in the Western Cape Province, South Africa

Tsitsi Bangira[a,b]*, Ben H.P. Maathuis[b], Timothy Dube[c] and Tawanda W. Gara[d]

[a]*Department of Geography and Environmental Studies, Stellenbosch University, Western Cape, South Africa;* [b]*Faculty ITC, Department of Water Resources, University of Twente, Enschede, The Netherlands;* [c]*Discipline of Geography, University of KwaZulu-Natal, Pietermaritzburg, South Africa;* [d]*Department of Geography and Environmental Science, University of Zimbabwe, Harare, Zimbabwe*

(*Received 27 March 2014; accepted 25 November 2014*)

The aim of the study was to evaluate flash flood potential areas in the Western Cape Province of South Africa, by integrating remote sensing products of high rainfall intensity, antecedent soil moisture and topographic wetness index (TWI). Rainfall has high spatial and temporal variability, thus needs to be quantified at an area in real time from remote sensing techniques unlike from sparsely distributed, point gauge network measurements. Western Cape Province has high spatial variation in topography which results in major differences in received rainfall within areas not far from each other. Although high rainfall was considered as the major cause of flash flood, also other contributing factors such as topography and antecedent soil moisture were considered. Areas of high flash flood potential were found to be associated with high rainfall, antecedent precipitation and TWI. Although TRMM 3B42 was found to have better rainfall intensity accuracy, the product is not available in near real time but rather at a rolling archive of three months; therefore, Multi- sensor precipitation estimate rainfall estimates available in near real time are opted for flash flood events. Advanced Scatterometer (ASCAT) soil moisture observations were found to have a reasonable r value of 0.58 and relatively low MAE of 3.8 when validated with *in situ* soil moisture measurements. The results of this study underscore the importance of ASCAT and TRMM satellite datasets in mapping areas at risk of flooding.

Keywords: topographic wetness index; satellite rainfall estimates; antecedent soil moisture; flash flood

1. Introduction

Among all kinds of natural hazards that occur globally, flooding is probably most devastating, wide spread and frequent (Mason et al. 1999; Groisman et al. 2005). The occurrence of natural hazards, mainly flash floods, has been on the rise in the past decades the world over. Flash floods occur at high intensity over a short-duration rainfall resulting in quick inundation. Flash floods have been responsible for the loss of life, infrastructure damage and destabilising the natural environment. As a result of increased frequency of flash floods, some areas are now classified as flash flood prone regions (Marchi et al. 2010). Scientists and meteorologists are of the view that most of these flash floods are a result of global warming and climate change (Mason et al.

*Corresponding author. Email: bangira26638@itc.nl

1999; Groisman et al. 2005). For instance, Mason et al. (1999) state that climate change triggers the occurrence of extreme weather events, by initiating rainfall of high intensity occurring within a short space of time resulting in devastating impacts on the environment (Murray & Ebi 2012). Flash floods are very difficult to predict mainly because they are characterized by quick and intense run-off generation that leads to rapid rise of water levels and high peak discharge over a short duration after the onset of the generating storm.

Current research indicates that in some parts of southern Africa particularly South Africa, Western Cape Province, there is an alteration of the magnitude, timing and spatial distribution of storms that produce extreme events (de Coning & Poolman 2011). For example, most of the well-known historical disastrous flash flood events have been recorded in 1968, 1970, 1981, 1987 and 2005 in most areas across South Africa. Recently, in July 2012, South African Weather Services (SAWS) reported that Cape Town, Cape Agulhas and Struisbaai received 70, 153 and 115 mm rainfall within a two-hour period, on 22 January 2009, respectively. These rainfall amounts have resulted in devastating impacts such as the destruction of settlements, valuable property and infrastructure. Based on this background, it is imperative to develop methods that are effective and reliable to characterize and monitor areas prone to these extreme weather events for planning and future management purposes. In this regard, key aspects such as extreme weather events, topography and physical characteristics of the catchments in such vulnerable areas are critical for the prediction, management and awareness purposes.

Currently, in South Africa, there are efforts to forecast potential flash floods using satellites technologies by studying and interpreting convective clouds (de Coning & Poolman 2011). Although this method has received notable attention, the approach does not account for the underlying hydro-meteorological conditions such as soil moisture (Petropoulos et al. 2014; Srivastava et al. 2014) and catchment geomorphological properties. Currently, knowledge on the utility of remote sensing technologies in identifying and mapping flash flood potential areas across Africa is still rudimentary. The use of remote sensing data-set can help in understanding vulnerable and potential areas at risk of flash floods across South Africa and the whole of Africa. Moreover, although flash floods account for the highest proportion of natural disasters, surprisingly little has been done in documenting their impacts at catchment scale in the Western Cape, South Africa (Faling et al. 2012). In this study, we therefore assume that embracing robust, quick and efficient new cutting edge remote sensing techniques can help in understanding and monitoring flash floods variability and distribution across the South Africa. The literature portrays remote sensing technologies as capable of providing (i) a better mapping alternative, given the extensive and complex nature of catchments, especially where routine field surveys are physically impossible (Chawira et al. 2013; Dube, Gumindoga, et al. 2014; Dube, Mutanga, et al. 2014; Petropoulos et al. 2014) (ii) the method offers a practical, timely and economical means of understanding the trends of flash floods (iii) its digital format sanctions fast processing of large data volumes, whereas the repeated acquisitions offer archive data useful for the detection of changes in flash floods over time, and (iv) its digital data can be easily integrated with ancillary data in a Geographic Information System (GIS) for further analysis. Unlike remote sensing, although gauges give relatively accurate point measurements of rainfall, they are associated with sampling errors in representing the areal rainfall over large areas. Moreover, the operation of gauges is costly, and in most cases, they are sparsely distributed and sometimes unavailable in remote areas. It is upon this background that

Borga et al. (2011), has recommended the use of remote sensing as an alternative means for estimating the rainfall field.

In order to compensate the problems of point rainfall estimation using rain gauges, researchers have thus shifted towards the use of satellite rainfall products. Satellite rainfall estimates offer a complete rainfall field when compared to point-based rainfall gauges. Even if gauge measurements are interpolated, they however offer a uniform rainfall field of despite it has a high spatial and temporal variability (de Coning & Poolman 2011). The use of satellite derived precipitation therefore allows the identification of extreme rainfall events both in spatial extent and magnitude (Asante et al. 2007). Nevertheless, Grimes et al. (1999) argued that satellite-based precipitation estimates should not replace gauge measurements but rather be a compliment to the rainfall field. Several studies have so far used remotely sensed datasets as inputs in hydrological models, to estimate stream flow during flash flood events. Sanyal and Lu (2004) did a flash flood management over the monsoon Asia by estimating flood depth using a digital elevation model (DEM). The study demonstrated that remote sensing and GIS can be used as the best tool for flash flood management in areas with limited resources, based on the topographic wetness index (TWI). Also, Asante et al. (2007) developed a flood monitoring model for the Limpopo river basin by parameterizing the Geospatial Stream Flow Model with remote sensed data-set coupled with *in situ* measurements. Similarly, their study highlighted the potential of satellite rainfall data-set and its importance in understanding water related problems (Asante et al. 2007). In this study, the assessment of flash flood potential areas (e.g. those only induced by high rainfall intensity) is done using remote sensing products based on the assumption that flash floods are a hydro-meteorological problem in accordance with Adeyewa and Nakamura (2003) and Borga et al. (2011).

This study is therefore intending for the first time to test the utility of remote sensing and accuracy in detecting patterns of high rainfall intensity that result in the occurrence of flash floods in the Western Cape Province of South Africa. The study is specifically based on two flash flood events that occurred in two different catchments around the Western Cape Province. Specifically, the main objective of this study was to evaluate the use of remote sensing and *in situ* data in mapping potential flash flood areas in selected catchments by integrating precipitation, topographic and soil wetness products.

2. Materials and methods

2.1. Study area

The study was conducted on Berg and Breede catchments found in the Western Cape Province, South Africa (Figure 1). The two catchments have an aerial coverage of approximately 3973 and 9864 km^2, respectively. Berg and Breede rivers flow south to north-west and north-west to south-east, respectively. The area is characterized by steep gradients with the highest being 2000 m a.s.l and the lowest being 40 m a.s.l. Mean annual precipitation in excess of 3000 mm in higher altitudes (upper part of the Berg catchment, Hottentots Holland Mountains) and less than 200 mm in low-lying areas (40 m a.s.l) (Bugan et al. 2012). The climate of the area is diverse mainly Mediterranean in nature with cold wet winters and hot dry summers. The climate is largely influenced by cold Atlantic Ocean and the warmer Indian Ocean along the coast of the Western Cape Province. Mean annual air temperature within the area range between 3.5 and 31 °C, with maximum recorded in December and minimum in July

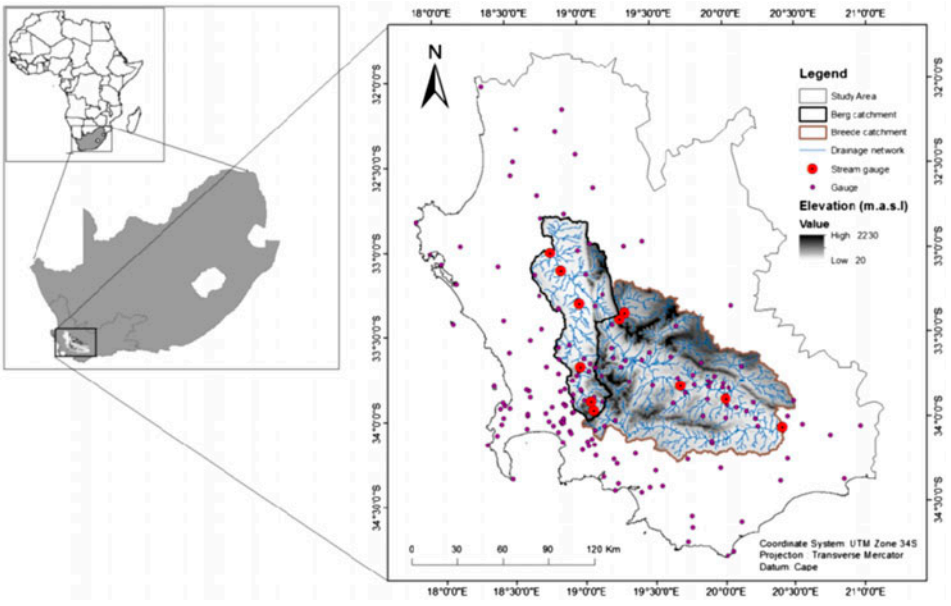

Figure 1. Study area, rainfall stations, stream gauges and Berg and Breede catchments at outlet G1H075 and H7H006, respectively.

(Bugan et al. 2012). Geologically, the area is dominated by Table Mountain Group sandstone in the high elevation areas and Malmesbury shale in the mid- to low-elevation parts. The soils are poorly developed, relatively shallow, brownish sandy loam soils with soil water-holding capacity of ±40% (Meadows & Hoffman 2003).

The catchments are characterized by heterogeneous land use and land cover. Most of the areas surrounding the catchments especially the Breede catchment, are covered by crops, pasture, vineyards and sparse vegetation. The vegetation type ranges from steppe, bush-grass savannah to succulent Karoo shrub lands. The catchments are also surrounded by cities as well as the informal settlements.

2.2. *Ground-based rainfall measurements data*

Ground-based rainfall measurements were obtained from the SAWS and Agricultural Research Council (ARC) of South Africa. The measurements are recorded through rainfall depth capturing using a tipping bucket method. The tipping bucket gauges can detect a minimum amount of 0.2 mm/h. Gauge data sets were obtained from SAWS and ARC at 60 min temporal resolution for 147 unevenly distributed stations. On the other hand; hourly stream flow data for the period 2008–2012 from 10 river gauges located on the main rivers of Berg and Breede were gathered from Department of Water Affairs of South Africa. Table 1 shows the stream gauge station names and the geographical location.

2.3. *Field measured data*

In situ data sets comprising the volumetric and gravimetric soil moisture measurement were collected in September 2012. Soil moisture measurements were done using a theta

Table 1. Stream flow gauging stations within the two catchments.

Gauge name	Latitude	Longitude	Gauge name	Latitude	Longitude
H1H003	33°22′50″S	19°18′06″E	G1H020	33°42′28″S	18°59′27″E
H1H006	33°25′18″S	19°16′01″E	G1H075	33°01′26″S	18°47′18″E
H4H017	33°49′05″S	19°41′35″E	G1H076	33°57′21″S	19°04′22″E
H5H004	33°53′52″S	20°00′42″E	G1H077	33°54′18″S	19°03′17″E
H7H006	34°04′03″S	20°24′20″E	G1H079	33°20′03″S	18°58′04″E

probe and soil measuring rings. The theta probes measure volumetric soil water content ($m^3\ m^{-3}$) based on the apparent water dielectric constant (Gaskin & Miller 1996). The measurements were mainly conducted in accessible and flash floods prone areas. The areas were initially determined from Google Earth and then validated using flash flood risk maps provided by the city of Cape Town. Sampled areas were then geo-coded using a global positioning system (GPS) at ±3 m accuracy. Sampling was then followed by the classification of these areas into a 200 × 200 m transects, totalling 15 transects. On each transect, 20 samples were conducted using a theta probe, with soil samples concurrently collected using soil rings. The 20 sampling measurements were then averaged. The average value was assumed to represent the entire transect. The points were then plotted on a scatter plot also removing outliers to ensure sampled data consistency. Thirty samples were collected from the core samples and put in zip lock plastics to prevent gain or loss of soil moisture.

$$\mathrm{MC}\,(\%) = \left(\frac{\mathrm{CSS} - \mathrm{ODS}}{\mathrm{DSW}}\right) \times 100 \tag{1}$$

where MC is the soil moisture content, CSS is the field collected soil samples in grams, ODS is the oven dried soils in grams and DSW is the dry soil weight in grams.

2.4. Remote sensing data products

Three satellite rainfall products, namely Tropical Rainfall Measuring Mission (TRMM 3B42), Multi-sensor Precipitation Estimate (MPE) and Climate Prediction Centre (CPC) Morphing method (CMORPH) and other satellite rainfall products (Rainfall Estimator (RFE), Africa Climatology (ARC2) and Tropical Applications of Meteorology using Satellite (TAMSAT) dekadal rainfall) were selected regarding their high spatial and temporal resolution as well as their coverage. MPE is a rain rate product of high temporal (15 min) and spatial (3 km) resolution, derived from the blending of high spatial and temporal resolution IR (10.5–12.5 μm) of the geostationary satellite data-set. CMORPH is a technique that produces complete global precipitation estimates by combining different passive microwave (PM) rainfall estimates from a variety of algorithms. At present, the CMORPH technique incorporates precipitation estimates derived from the PMs aboard the Defence Meteorological Satellite Programme 13, 14 and 15 (Special Sensor Microwave Imager (SSM/I)), the National Oceanic and Atmospheric Administration (NOAA)-15, 16, 17 and 18 (Advanced Microwave Sounding Unit: AMSU-B), and The Advanced Microwave Scanning Radiometer-EOS (AMSR-E) and the TRMM Microwave Imager (TMI) aboard the National Aeronautics and Space Administration Aqua and TRMM spacecraft, respectively.

Other satellite rainfall products used in this study include the RFE developed by the CPC of NOAA, to monitor hydrological trends in support of the humanitarian aid

programmes of Famine Early Warning Systems Network (FEWS-NET) and TAMSAT dekadal rainfall produced by University of Reading, United Kingdom. RFE product blends local regional gauge with SSM/I and AMSUB satellite rainfall estimates at a high spatial resolution of 0.1° on a near real time basis to provide daily rainfall estimates over Africa (Novella & Thiaw 2012). TAMSAT dekadal rainfall product integrates thermal infrared imagery of Meteosat satellite data with local ground-based observations over Africa at a 10 day and 4 km temporal and spatial resolution.

Soil moisture estimates were derived from Advanced Scatterometer (ASCAT) and validated with ground soil moisture measurements. ASCAT sensor estimates soil moisture based on C band at a spatial resolution of 25 km resampled to 12.5 km resolution. ASCAT soil moisture estimates product has been reported in the literature to have a high correlation with *in situ* measurements (Brocca et al. 2011).

2.5. *Remotely sensed data pre-processing*

Satellite and ground rainfall measurement data products were resampled and aggregated to same temporal and spatial resolutions of three h and 8 km, respectively. Satellite rainfall data were extracted for points that coincided with gauged rainfall measurements using a 3 × 3 kennel window using ILWIS 3.7 Interface. In order to achieve the above objective, gauged rainfall data obtained from SAWS and ARC at 60 min temporal resolution for 147 unevenly distributed stations was screened to 90 for extreme events. Data from stations that had redundancy, missing values, and showed some inconsistency with stations in its proximity were discarded. Hourly gauge data were summed to three hourly time steps and to daily time step for comparison with satellite rainfall. The most important point that was put into consideration was the time difference between the South African Local Sidereal Time (LST) and Coordinated Universal Time (UCT). South African time is GMT +2, so as a result, gauge data were compiled based on two hours ahead. Thus, three hourly gauge rainfall is defined as total for three consecutive hours beginning at 0000 UTC (0200 LST) for a given day. The three hourly time steps were chosen as proposed by Crosson et al. (1996). No changes to gauge data were done except the elimination of gauging stations with significant errors. Thus, only nine stations in the vicinity of each catchment with good quality data were used for the merging of satellite and gauge measurements. In addition, for satellite comparison, all gauges in the vicinity of the sub catchments were averaged such that there was one gauge at eight km pixel, for easy comparison with satellite products.

2.6. *Satellite rainfall data pre-processing*

Analysis was done only for the rainy months of May, June, July and August from 2008 to 2012. Fifteen minutes satellite precipitation estimates from MPE were aggregated to three hourly to match the temporal resolution of CMORPH and TRMM 3B42. Later, all the products were aggregated to daily time step to get the idea on whether correlation improves at increased time step and also for calculation of rainfall using daily climatological RFE ARC 2 product.

CMORPH, MPE and TRMM-3B42 precipitation estimates for gauge locations were retrieved in two ways as elaborated by Crosson et al. (1996), namely (a) Gauge locations superimposed on SRE pixels and the pixel value that coincides with the gauge location (b) The mean rainfall over 3 × 3 pixel kernel (24 km × 24 km) regions centred at the gauge point of geo location. The later averaging method was done to minimize

the errors associated with timing, image geo-location and wind driven rain shifts. The earlier method was chosen because a derived point value from the satellite has higher accuracy when compared to the pixel value from point interpolation method. Kernel size was chosen based on the assumption that 24 km is almost close to the original pixel size of the TRMM 3B42 and CMORPH before resampling.

The processed two tiles of 5° by 5°, 90 m Shuttle Radar Topography Mission Digital Elevation Model (SRTM DEM) were imported into Integrated Land and Water Information System (ILWIS) using In-situ and Online Data toolbox. A GIS-based algorithm called DEM hydro-processing in ILWIS, (Maathuis & Wang 2006), was used to extract the Berg and Breede catchments and analyse their geomorphological characteristics and river paths. Extracted catchments were further processed to derive compound parameters such as TWI.

2.7. Combining gauge measurements with satellite estimates

Matching co-located three hourly gauge and satellite rainfall estimates (CMORPH, MPE and TRMM 3B42) at 8 km spatial resolution data were extracted for two extreme events that occurred in two different catchments. The extreme events considered were the 11–13 July 2009 and 11–13 August 2012. Curves were drawn through cumulative point measurements of the three hourly pairs. Resulting gauge and respective SRE plot suggested that a quadratic regression function was the most appropriate because of high correlation and low standard error as compared to the linear fitting. The quadratic equations show a high correlation and a low standard error of estimate as compared to the linear equations. Moreover, the size of the coefficients a, b and c were minimum. The curve expert software was used to calculate the coefficients of the regression fit as well as the standard error of estimate. Cumulative curves for the satellites were each fitted to the gauge cumulative curve. This was done based on the assumption that gauge measurements are unbiased or have minimum errors as compared to satellite estimates. Xie and Arkin (1995) have indicated that gauge-based analyses are less biased when there is at least one station over grid boxes of 0.25°.

2.8. Topographic wetness index

TWI is calculated using representative points based on the assumption that the points in the catchment with the same range of topographic index will have same hydrological responses (Beven & Kirkby 1979). TWI is defined by the equation below:

$$\mathrm{TWI} = \ln\left(\frac{a}{\tan\beta}\right) \tag{2}$$

where a is the source contributing area, and $\tan\beta$ is ground surface slope.

TWI was derived from the DEM directly through the hydro-processing algorithm in ILWIS based on the above equation. Computation of a in ILWIS was based on a single flow direction, D8 flow direction algorithm. The algorithm assumes that all water from the central pixel should flow into one of the surrounding neighbouring pixel with the lowest elevation or steepest slope. The flow is partitioned to all downslope neighbouring cells. The maximum downslope gradient is used to approximate $\tan\beta$ for TWI. Higher values of TWI indicate areas more likely to drain by saturated excess flow.

2.9. Selection of rainfall events and subcatchments

Two flash flood events were selected in this study based upon the gauge measurements for the time period May to August of the years 2008–2012. Characteristics of flash flood events as explained by Marchi et al. (2010) were used as a working principle for selecting two flash flood events. These include duration of the causative rainfall limited to 34 h, the response time of the catchment, peak discharge and the severity of the event. The two selected events are 12 July 2009 and 11 August 2012 which have occurred in catchments along the main rivers of Berg and Breede. The second criterion used was based on observation of catchments where flash flood events had occurred. The catchment size made to cater for the coarse resolution of the satellite products such as TMI for soil moisture which had a 25-km spatial resolution. Differences between the spatial extents of the catchments and time of the season during which the flash floods had occurred were also put into consideration during the selection of the rainfall events. The selected catchments also involved field observed stream discharge data at selected points given (Table 1 and Figure 1).

2.10. Determining flash flood potential areas by integrating remote sensing products

The flash flood index was developed to show potential areas for flash flooding by integrating high spatial and temporal resolution remote sensing rainfall, soil wetness and topographic data. After developing all raster gridded datasets that represent hydro-physiographic characteristics that influence flash flood, these maps were resampled to a consistent resolution using the nearest neighbour resampling method. The maps were classified into discrete dimensionless classes of 1, 2 and 3 based on class threshold values of neighbouring pixels. High values were assigned to high hierarchy classes. Considering two rainfall events and three satellite rainfall products, six maps in total were produced at final stage.

2.11. Combining rainfall anomaly, TWI and SWI

The static layer of slope in the form of TWI was combined to dynamic event layers of rainfall anomaly by the use of weights. Without first observing each map, it was difficult to assign the weight values for combining the maps; therefore, the maps were first qualitatively studied.

Three hourly gauge corrected satellite rainfall were accumulated and averaged to daily to match with the RFE daily climatological average. Since these events were considered for 36 h, only the actual day of the event with high rainfall was chosen for this process. Thus, only 12 July 2009 and 11 August 2012 were considered for Berg and Breede catchments, respectively. Rainfall anomaly was calculated by finding the difference between the gauges corrected satellite rainfall and the climatological daily average rainfall. Positive anomaly shows the potential for flooding, whereas negative reveal that lower than average rainfall was received. The anomaly maps were corrected for negative values and combined to TWI map. Rainfall was given much weight because it is the initiator for flash floods. They were combined using the calculations below:

$$\text{Combined rainfall anomaly and TWI} = 2(\text{rainfall anomaly}) + 0.5(\text{TWI}) \qquad (3)$$

The weights of the equation were based on the trial and error basis. On the other hand, ASCAT soil wetness was combined to the negatively corrected Normalised Difference Wetness Index (NDWI) infrared images. McFeeters (1996) have explained that NDWI

makes use of reflected near-infrared radiation and visible green light to enhance the presence of wet features while eliminating the presence of soil and terrestrial vegetation. The NDWI was given much weight of 0.6, whereas ASCAT 0.4 because NDWI was subjectively determined as a less bias regional product, so it is less susceptible to local errors. Finally, the maps were joined to one product with the soil wetness index (SWI) getting less weight. Rainfall and slope maps were much overweighed compared with soil wetness maps due to the fact that rainfall and topography are the major contributing factors for flash flooding (Marchi et al. 2010). This argument has been adopted from the study by Doswell et al. (1996) who concluded that even in dry soil conditions flash floods have been witnessed; hence, the hydrological characteristics of the basin may be the most important considerations. Since the NDWI, ASCAT and TRMM had a mismatch in terms of spatial size, the datasets were resampled to a similar pixel size using the nearest neighbour resampling technique in a GIS environment.

3. Results and discussion

3.1. Temporal trends in gauge measured rainfall

Based on 90 unevenly distributed rainfall stations, temporal rainfall trends for the period 2008–2012 were analysed. Monthly average for each station was calculated using arithmetic mean and assumed to represent areal average surrounding the gauge. All the events with rainfall intensity greater than 30 mm per hour were categorized as extreme events. Frequency of these extreme events for the period 2008–2012 for the 90 stations was analysed. July has the highest frequency of rain events of greater than 30 mm per hour, and December has the least. It is also interesting to note that November has also a number of extreme events even though it is not a rainy season month. Inverse distance weighting (IDW) interpolation method was used to show spatial distribution of rainfall in the area. IDW gives more weight to areas which are close to the interpolated point. Although flash floods are caused by extreme events, mean annual spatial variability of rainfall gives information on the amount of rainfall the catchment is adapted to (Figures 2 and 3).

Vergelegenvrug station recorded the most intense rainfall event of 180.4 mm within one hour on 3 March 2009 at 1400 h. Struissbai recorded the second and Cape Agulhas recorded the third with 89.8 mm and 81.2 mm on 22 January 2009, respectively. All the three stations are close to the coast at low elevation. Therefore, the major cause for these rainfall events could have been due to ‘cut-off low’ pressure systems. Stations which are close to the coast and on high elevation are on average those that receive large amount of rainfall as compared to those that are interior. Per year analysis of the extreme events, 2009 was found to have recorded the most intense extreme events. It was also observed that although, the winter months have the greatest frequency of extreme events, many of the events of greatest intensity occur outside winter months.

Extreme events of 11–13 July 2009 and 11–13 August 2012 were also selected from these graphs by considering peak discharge and shape of storm hydrographs. As can be seen in the graphs, both of the events,` hydrograph shape, have steep rising limbs with short duration, typical of flash flood events. Steep rising limbs of the storm hydrographs can also explain the characteristics of the catchments in terms of run-off generation and speed of its flow to low-lying areas. Furthermore, the hydrographs reproduced the rainfall patterns shown by all satellite observations and gauge measurements.

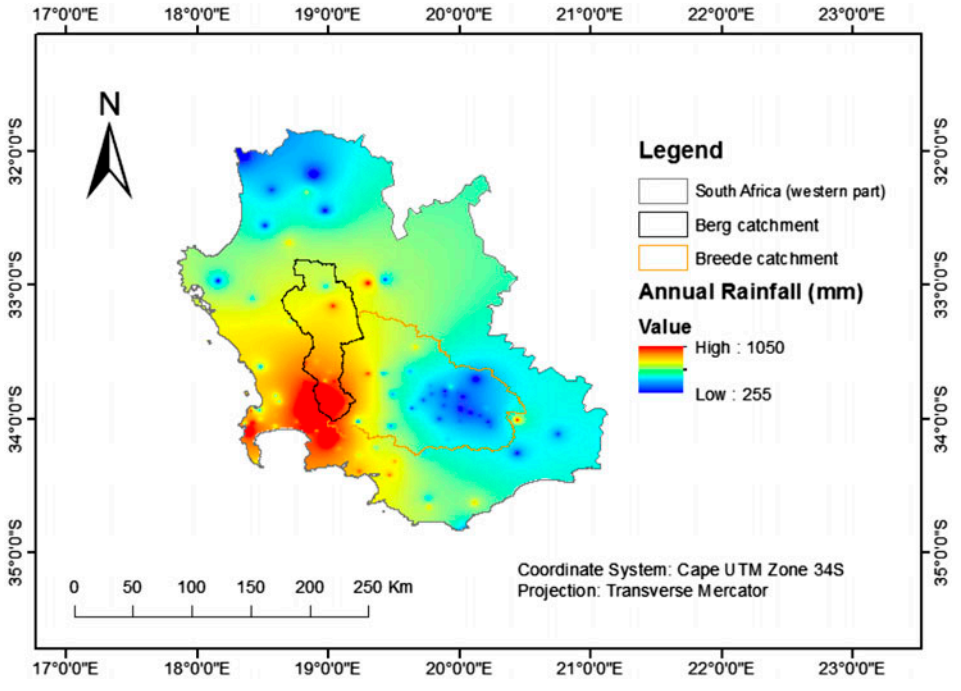

Figure 2. Rainfall intensities of extreme events.

Considering per catchment analysis in terms of stream hydrographs response curves, Breede catchments generate run-off even with minimum rainfall received as compared to Berg catchment. This clearly indicates different morphometric properties of these catchments. On the another hand, it can be argued that Berg catchment is adapted to high rainfall intensities such that the same amount of rainfall in Berg catchment can cause large amounts of run-off in Breede catchment.

Impact of antecedent soil wetness in relation to run-off generation can also be seen in these graphs especially Breede graphs (Figure 4). When there was rain in some few days before intense rainfall, the peak of the resultant discharge graph is very high. This is so because the soils will only allow minimum amount of rainfall to infiltrate before they are saturated and the excess will be run-off. Overestimation of TRMM3B42 can also be explained by comparing its rainfall estimates with run-off generation. For example on the dates of around 20 July 2012 (Figure 4), it estimated high amounts of rainfall and the resultant run-off was not much as compared to that one of around 26 June 2012.

All the products on the selected two extreme events showed good positive correlation with the calculated r value of 0.61 from CMORPH at three hourly time step and the highest being 0.91 from TRMM 3B42 at a daily time step as shown in Figure 5. TRMM 3B42 has an improved r with about 15% from three hourly time step to daily. Furthermore, the correlation coefficients of all the comparisons are positive, meaning that the increase in the gauge measurements results also in the high values being estimated by the satellites.

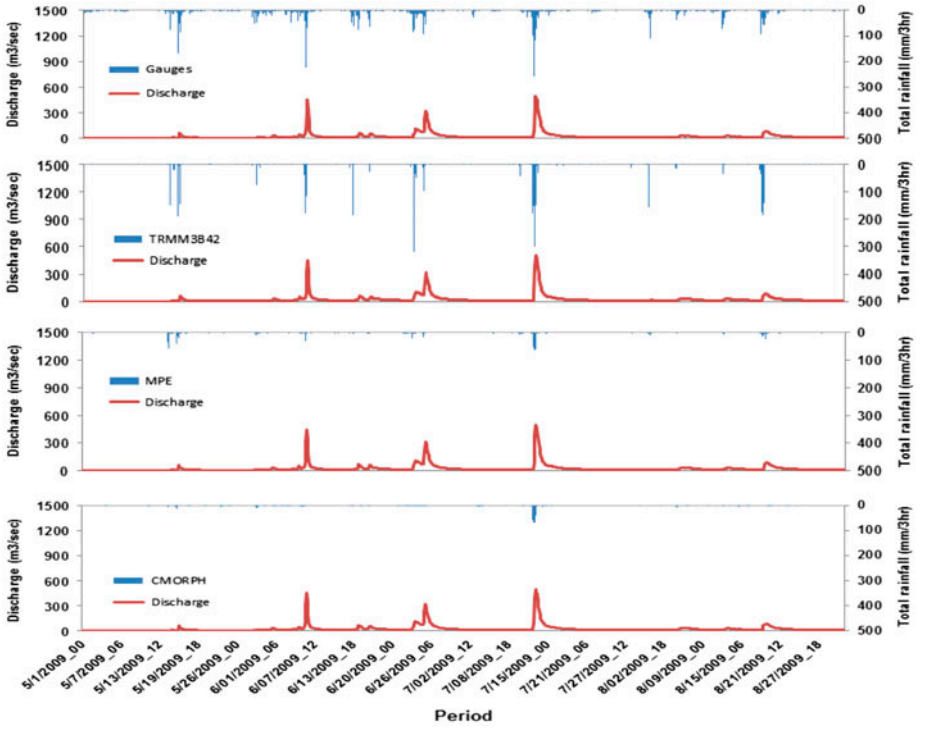

Figure 3. Measured discharge at G1H075 and rainfall trend from gauge and satellite estimates over Berg catchment for the rain season of 2009.

Heinemann and Kerenyi (2003) concluded that MPE algorithm is only suitable for convective weather situations and also Liechti et al. (2012) found that CMORPH has strong negative bias when it was compared with gauges along the Zambezi basin. Frontal rainfalls such as the one that occur in Western Cape of South Africa seem to be wrongly located and underestimated by MPE and CMORPH.

Further evaluation of the three hourly rainfalls over the two catchments was carried out by calculating average accumulated areal rainfall for each rainfall season over the years 2008–2012 based on nine stations. In both Breede and Berg areal rainfall; TRMM 3B42 was found to have the highest ratio of 0.89 and 0.84, respectively. In line with the findings of this study, Islam et al. (2012) have found a high correlation of 0.91 between attenuation corrected reflectivity from TRMM precipitation radar with measured reflectivity from ground-based radars. CMORPH was found to have the lowest ratio with values of 0.24 in the Berg and 0.34 in the Breede. The higher the ratio the more close the satellite estimates are to the gauges.

3.2. Climatological analysis of the extreme events

Climatological RFE daily mean from 1983 to 2012 was used to give a better representation of the trend of abnormal wetter and drier conditions in the Western Cape of South Africa (Figure 6). The difference between daily TRMM 3B42, MPE and

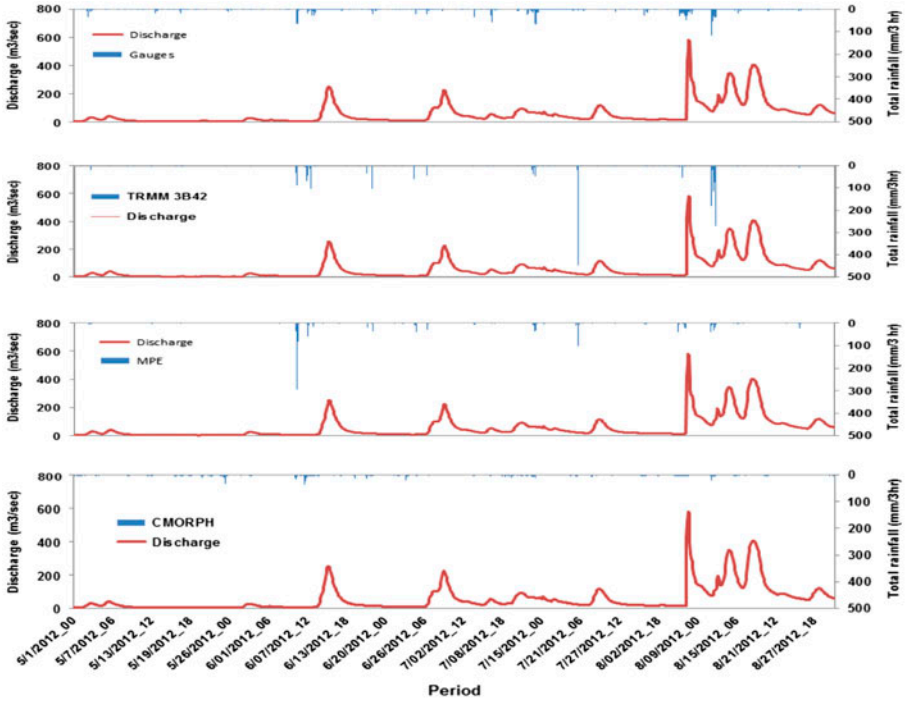

Figure 4. Measured discharge at H7H006 and rainfall trend from gauge and satellite estimates over Breede catchment for 2012 rain season.

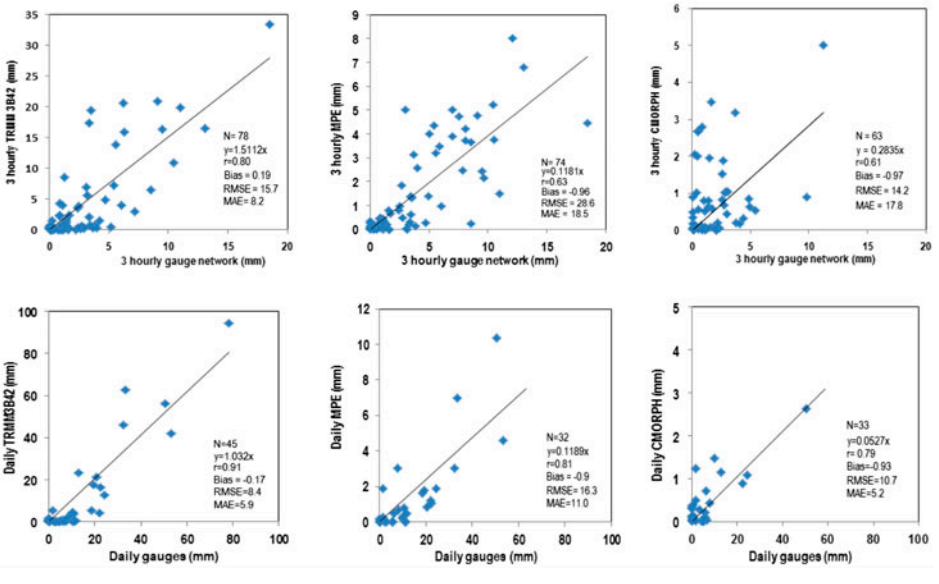

Figure 5. Scatter diagrams of 3 hourly (top) and daily (bottom) satellite rainfall estimates paired with gauge measurements for the rain season of 2009.

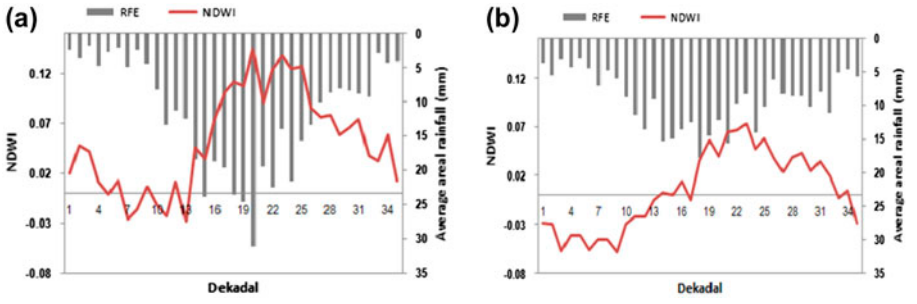

Figure 6. Climatological dekadal RFE and NDWI in (a) Berg and (b) Breede catchments.

CMORPH with RFE mean, daily climatological was used to calculate the daily anomaly. Even though the anomaly is not an index, it can show the trend of wetter and drier than normal conditions as shown in Figure 5. Negative anomaly shows drier conditions, whereas on the other hand, positive values indicate wetter conditions. Anomaly measurements were plotted together with discharge to get a more understanding on the peaks and shape of the discharge curves during wet conditions in the Berg and Breede catchments. The response of the catchments is very different as seen by the relationship between discharge and rainfall anomaly. Breede catchment produces much run-off with minimum amount of rainfall received. This could be because of different catchment morphometric properties which are going to be explained in sections to follow. Furthermore, discharge curves in both catchments are controlled by antecedent precipitation. Figure 5 shows that TRMM 3B42 and gauges can depict almost all the flash floods, but CMORPH and MPE can depict trend although they underestimate extreme rainfall events as shown in Figure 5. The highest anomaly was recorded in July for Berg catchment and for Breede catchment was recorded in August. Therefore, flash floods are more likely to occur during these months in the respective catchments.

The comparison of NDWI was compared with dekadal climatological RFE ARC2 results indicate a similar trend in terms of surface wetness as presented in Figure 6. The highest peak in the Berg catchment occurs on 12 July 2009 while on the other hand; the one on 11 August 2012 (e.g. in Breede catchment) has a slightly higher anomaly and NDWI. The RFE ARC2 also shows that Berg catchment receives much more rainfall when compared to Breede, hence high occurrence of flash floods. When rainfall is high, NDWI is positive; therefore, high rainfall intensity is likely to contribute to a flash flood occurrence on the areas with high NDWI.

3.3. *Validation of ASCAT surface soil moisture product*

The overpass of 28 September during 2057 h was used to validate the ASCAT soil moisture. The volumetric *in situ* measurements were converted to percentage soil moisture for easy analysis with the ASCAT SWI. ASCAT soil moisture product was validated with *in situ* soil moisture measurements collected during fieldwork at a depth of 0–10 cm for 10 sites. The measurements conducted between 19 and 23 September 2012 were discarded because the satellite did not cover the study area. The product shows a low MAE of 3.8, $r = 0.58$ and bias of −6%. The negative bias reveals that the ASCAT soil moisture product underestimates the actual soil moisture. The plot of the results as well as the image used for validation is shown in Figure 7. The results

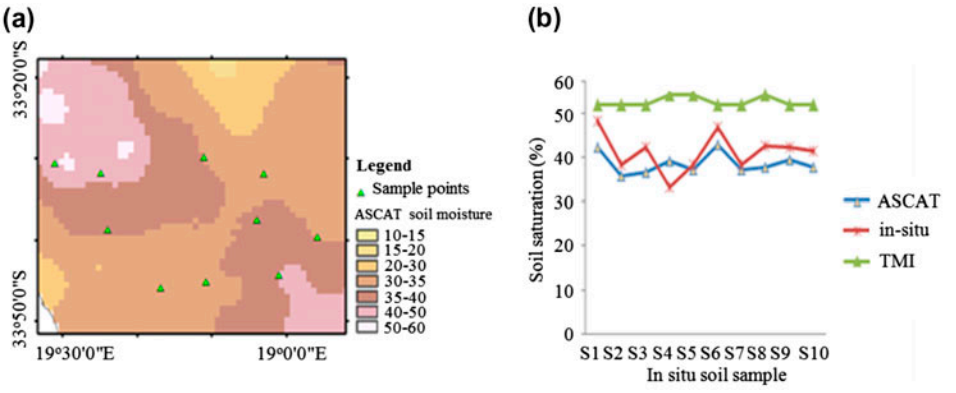

Figure 7. (a) ASCAT inverse distance interpolated images of 28/09/201(2054 and 2057 h) used for validation and (b) validation results.

are supported by the outcomes of Sinclair and Pegram (2010); they found higher correlation between ASCAT products with *in situ* measurements in KwaZulu-Natal of South Africa.

3.4. *Combined TWI, rainfall anomaly and SWI*

Results of daily rainfall anomaly maps for 12 July 2009 and 11 August 2012 which were generated from the difference between daily mean climatological RFE and satellite corrected daily mean are presented in Figure 8. Point to note is that each map was classified into 5 classes basing on its minimum and maximum anomaly. All the satellite products estimated high rainfall amounts close to the coast for 12 July 2009, resulting

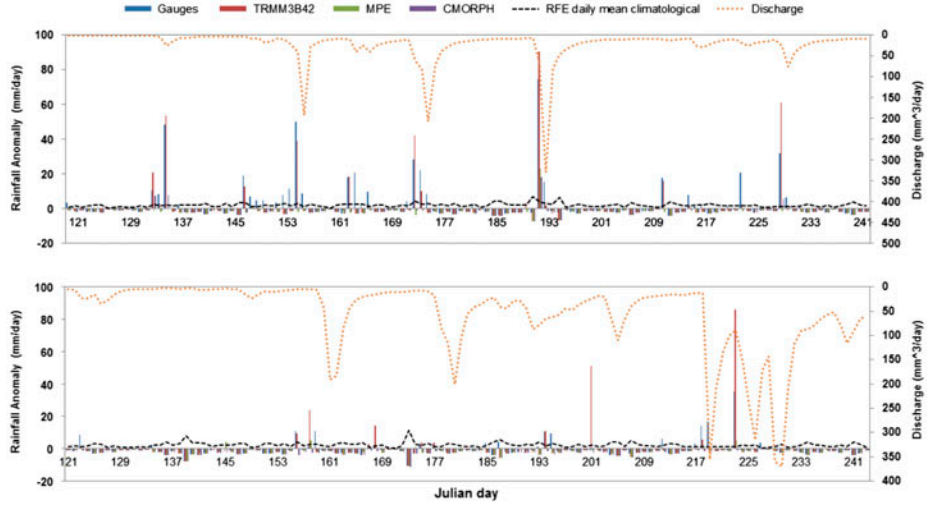

Figure 8. Daily mean climatological RFE and anomaly over Berg (top) and Breede (bottom) catchments for the rainfall season of 2009 and 2012 at stream gauges G1H0075 and H7H006.

in high anomalies also in these areas. However, for the 11 August 2012 event, TRMM3B42 recorded highest rainfalls in the interior around the Breede catchment. The results of these rainfall anomaly maps are in accordance with interview results from the relevant agents about areas prone to flash flooding. Furthermore, there was also high rainfall in the catchments which were captured by all the satellite products respective of the day of the event and where the flash flood had occurred.

Figure 9 shows the final product of flash flood potential areas. Potential areas were classified into four classes based on their ability to generate high and efficient run-off, antecedent wetness soil moisture and high rainfall intensity. Areas which have an extreme potential to flash flooding have an index from 0.8 to 1, and the least have an index between 0 and 0.2. Most of these areas are those which are close to the coast as shown by the 12 July 2009 event. These results are in support to what Midgley et al. (2005) got in their study for the assessment of climate change in the Western Cape Province. CMORPH and MPE estimates for the event of 12 July 2009 show almost the same areas which have high potential for flash flooding. On this day, TRMM 3B42 misses some of the interior rainfall which was captured by CMORPH and MPE. During the 11 August 2012, event all the satellite products picked the rain estimates of this event. This could be because the event occurred almost at the end of the winter season and could have been of convection type and not of cut-off low pressure systems.

However, although this study has shown that rainfall is one of the major factors responsible for initiating flash flood, this is not always the case the world over. Other factors such as slope, geology, vegetation cover and geomorphology are important factors for causing flash flood events (Bradshaw et al. 2007). For instance, the complex interplay of factors such as rainfall variability, altitude and distance to the coast, catchment steepness, soil depth, the degree of disturbance to undergrowth and soil, and soil fertility and their relative importance play a critical role in determining the occurrence of flash floods (Bruijnzeel 2004; Bradshaw et al. 2007 Alila et al. 2009; Coe et al. 2009).

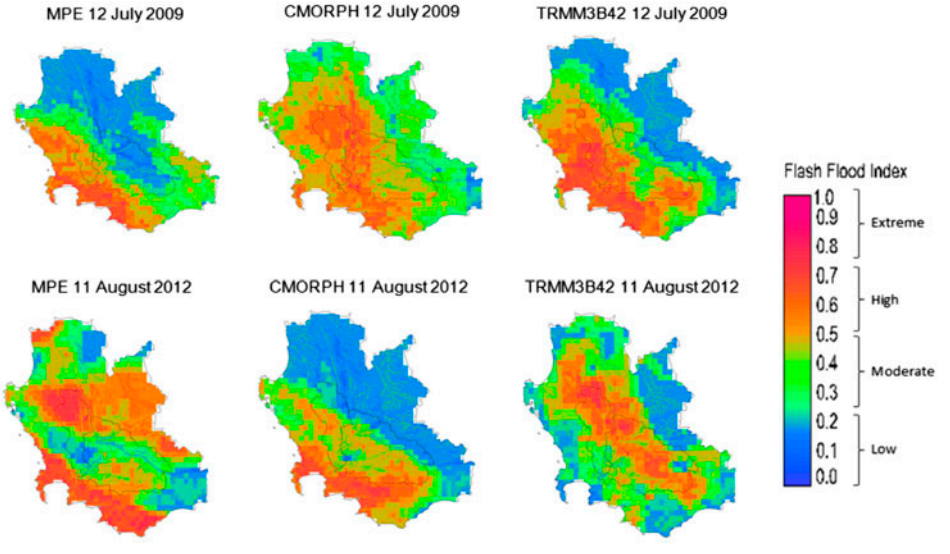

Figure 9. Flash flood potential areas based on TWI, antecedent soil moisture and rainfall anomaly on 12 July 2009 and 11 August 2012.

4. Conclusions

High rainfall intensity of short duration on saturated soils as well as on steep slopes favours flash flood potential. The integration of spatial layers of all the favourable characteristics for flash flooding results in the mapping of flash flood potential areas in the Western Cape of South Africa. The focus of this study was to improve the accuracy of satellite rainfall fields by correcting for their bias with local gauge measurements before they are further integrated with antecedent soil moisture and TWI for mapping of flash flood potential areas. Therefore, the impacts of flash floods can be reduced using near real time satellite products such as MPE to predict their occurrence. However, based on the objectives and research questions of this study, the following conclusions and findings were drawn.

Gauge measurements analysis

- July has the highest amount of extreme rainfall events greater than a threshold value of 30 mm per hour and also receives high rainfall. January has the least in both amount of rainfall and frequency of extreme events.
- Rainfall decreases from south to north and east to west mainly because of topography, warm and wet coastal winds that promote rain bringing clouds.
- There is a great difference in rainfall variability between stations which are in close proximity to each other. Berg catchment receives much rainfall as compared to Breede catchment.

Comparison between gauge and satellite rainfall products

- This study has shown that high temporal resolution satellite products namely TRMM 3B42, CMORPH and MPE are suitable for estimating extreme rainfall events. Generally speaking, the three satellite rainfall products studied here provide similar qualitative spatial distribution patterns of rainfall with different magnitudes of rainfall intensities. Higher correlation shows good timing as well as capturing of high rainfall intensities by both gauge and satellite data sources. TRMM 3B42 slightly overestimates at both three hourly and daily time scales compared with gauges but has a low bias.
- However, the accuracy improved for all satellite products as the integration time step increases from three hourly to daily and seasonal. This improvement shows that even at higher temporal resolutions something can be done to improve satellite rainfall estimates for extreme rainfall prediction.

Validation of ASCAT soil moisture product

- ASCAT soil moisture product has low bias as compared to *in situ* measurements; hence, it can be used for temporal and spatial monitoring of antecedent precipitation. However, long-term continuous ground measurement and detailed analysis are needed to support these results.

Flash flood potential areas

- Flash flood potential areas of the Western Cape of South Africa in the selected catchments can be demarcated by integrating remote sensing products. Areas with

greatest potential for flash flooding where found to be those that have received high rainfall when the antecedent soil moisture was high and have steep slopes that increase the kinematic flow of run-off to low contributing areas. Topography, antecedent moisture as well as high rainfall intensity promotes flash floods.

Acknowledgments

Authors would like to thank the South African Weather Services (SAWS) and Agricultural Research Council of South Africa (ARC) for providing hourly rainfall data. Many thanks also go to the City of Cape Town Rapid Response Disaster Risk Management for providing maps of flash flooding risk areas. South Africa's Department of Water Affairs is acknowledged for providing hourly stream gauge measurements for the Breede and Berg rivers. Finally, the University of the Western Cape, Department of Environmental & Water Science for being resourceful during data collection.

Disclosure statement

No potential conflict of interest was reported by the authors.

References

Adeyewa ZD, Nakamura K. 2003. Validation of TRMM radar rainfall data over major climatic regions in Africa. J Appl Meteorol. 42:331–347.

Alila Y, Kuraś PK, Schnorbus M, Hudson, R 2009. Forests and floods: a new paradigm sheds light on age-old controversies. Water Resour Res. 45:1–24.

Asante KO, Macuacua RD, Artan GA, Lietzow RW, Verdin JP. 2007. Developing a flood monitoring system from remotely sensed data for the Limpopo basin. IEEE Trans Geosci Remote Sens. 45:1709–1714.

Beven, KJ, Kirkby, MJ. 1979. A physically based, variable contributing area model of basin hydrology. Hydrol Sci Bull. 24:43–69.

Borga M, Anagnostou EN, Blöschl G, Creutin JD. 2011. Flash flood forecasting, warning and risk management: the HYDRATE project. Environ Sci Policy. 14:834–844.

Bradshaw CJ, Sodhi NS, Peh KSH, Brook BW. 2007. Global evidence that deforestation amplifies flood risk and severity in the developing world. Global Change Biol. 13:2379–2395.

Brocca L, Hasenauer S, Lacava T, Melone F, Moramarco T, Wagner W, Bittelli M. 2011. Soil moisture estimation through ASCAT and AMSR-E sensors: an intercomparison and validation study across Europe. Remote Sens Environ. 115:3390–3408.

Bruijnzeel LA. 2004. Hydrological functions of tropical forests: not seeing the soil for the trees? Agric Ecosyst Environ. 104:185–228.

Bugan RDH, Jovanovic, NZ, De Clercq WP. 2012. The water balance of a seasonal stream in the semi-arid Western Cape (South Africa). Water SA. 38:201–212.

Chawira M, Dube T, Gumindoga W. 2013. Remote sensing based water quality monitoring in Chivero and Manyame lakes of Zimbabwe. Phys Chem Earth, Parts A/B/C. 66:38–44.

Coe MT, Costa MH, Soares-Filho BS. 2009. The influence of historical and potential future deforestation on the stream flow of the Amazon River-Land surface processes and atmospheric feedbacks. J Hydrol. 369:165–174.

Crosson WL, Duchon CE, Raghavan R, Goodman SJ. 1996. Assessment of rainfall estimates using a standard Z-R relationship and the probability matching method applied to composite radar data in Central Florida. J Appl Meteorol. 35:1203–1219.

de Coning E, Poolman E. 2011. South African Weather Service operational satellite based precipitation estimation technique: applications and improvements. Hydrol Earth Syst Sci. 15:1131–1145.

Doswell CA, Brooks HE, Maddox RA. 1996. Flash flood forecasting: an ingredients-based methodology. Wea Forecasting. 11:560–581.

Dube T, Gumindoga W, Chawira M. 2014. Detection of land cover changes around Lake Mutirikwi, Zimbabwe, based on traditional remote sensing image classification techniques. Afr J Aquat Sci. 39:89–95.

Dube T, Mutanga O, Elhadi A, Ismail R. 2014. Intra-and-inter species biomass prediction in a plantation forest: testing the utility of high spatial resolution spaceborne multispectral rapideye sensor and advanced machine learning algorithms. Sensors. 14:15348–15370.

Faling W, Tempelhoff JWN, van Niekerk D. 2012. Rhetoric or action: are South African municipalities planning for climate change? Dev South Afr. 29:241–257.

Gaskin GJ, Miller JD. 1996. Measurement of soil water content using a simplified impedance measuring technique. J Agric Eng Res. 63:153–159.

Grimes DIF, Pardo-Iguzquiza E, Bonifacio R. 1999. Optimal areal rainfall estimation using raingauges and satellite data. J Hydrol. 222:93–108.

Groisman PY, Knight RW, Easterling DR, Karl TR, Hegerl GC, Razuvaev VAN. 2005. Trends in intense precipitation in the climate record. J Clim. 18:1326–1350.

Heinemann T, Kerenyi J. 2003. Eumetsat multisensor precipitation estimate (MPE): concept and validation. [cited 2013 Jan 1]. Available from: http://www.eumetsat.int/groups/ops/documents/document/mpe_conceptvalidation_uc2003.pdf

Islam T, Rico-Ramirez MA, Han D, Srivastava PK, Ishak AM. 2012. Performance evaluation of the TRMM precipitation estimation using ground-based radars from the GPM validation network. J Atmos Sol Terr Phys. 77:194–208.

Liechti TC, Matos JP, Boillat JL, Schleiss AJ. 2012. Comparison and evaluation of satellite derived precipitation products for hydrological modeling of the Zambezi River Basin. Hydrol Earth Syst Sci. 16:489–500.

Maathuis, BHP, Wang, L. 2006. Digital elevation model based hydro-processing. [cited 2013 Jan 17]. Available from: http://www.geocarto.com.hk/cgi-bin/pages1/mar06/3_Maathuis.pdf

Marchi L, Borga M, Preciso E, Gaume E. 2010. Characterisation of selected extreme flash floods in Europe and implications for flood risk management. J Hydrol. 394:118–133.

Mason SJ, Waylen PR, Mimmack GM, Rajaratnam B, Harrison JM. 1999. Changes in extreme rainfall events in South Africa. Clim Change. 41:249–257.

McFeeters SK. 1996. The use of the normalized difference water index (NDWI) in the delineation of open water features. Int J Remote Sens. 17:1425–1432.

Meadows ME, Hoffman TM. 2003. Land degradation and climate change in South Africa. Geog J. 169:168–177.

Midgley GF, Chapman RA, Hewitson B, Johnston P, de Wit M, Ziervogel G, Forsyth GG. 2005. A Status Quo, vulnerability and adaptation assessment of the physical and socio-economic effects of climate change in the Western Cape. Report to the Western Cape Government. Cape Town (South Africa): CSIR Report No. ENV-S-C 2005-073, Stellenbosch.

Murray V, Ebi KL. 2012. IPCC special report on managing the risks of extreme events and disasters to advance climate change adaptation (SREX). J Epidemiol Community Health. 66:759–760.

Novella NS, Thiaw WM. 2012. African rainfall climatology version 2 for famine early warning systems. J Appl Meteorol Climatol. 52:588–606.

Petropoulos GP, Ireland G, Srivastava PK, Ioannou-Katidis P. 2014. An appraisal of the accuracy of operational soil moisture estimates from SMOS MIRAS using validated in situ observations acquired in a Mediterranean environment. Int J Remote Sens. 35:5239–5250.

Sanyal J, Lu XX. 2004. Application of remote sensing in flood management with special reference to Monsoon Asia: a review. Nat Hazards. 33:283–301.

Sinclair S, Pegram GGS. 2010. A comparison of ASCAT and modelled soil moisture over South Africa, using TOPKAPI in land surface mode. Hydrol Earth Syst Sci. 14:613–626.

Srivastava PK, Han D, Rico-Ramirez MA, O'Neill P, Islam T, Gupta M. 2014. Assessment of SMOS soil moisture retrieval parameters using tau–omega algorithms for soil moisture deficit estimation. J Hydrol. 519:574–587.

Xie PP, Arkin PA. 1995. An intercomparison of gauge observations and satellite estimates of monthly precipitation. J Appl Meteorol. 34:1143–1160.